ACS Photonics

pubs.acs.org/journal/apchd5

Article

Saturation Mechanisms in Common LED Phosphors

Marie Anne van de Haar,* Mohamed Tachikirt, Anne C. Berends, Michael R. Krames, Andries Meijerink, and Freddy T. Rabouw*

Cite This: *ACS Photonics* 2021, 8, 1784−1793

Read Online

ACCESS | Metrics & More | Article Recommendations | Supporting Information

ABSTRACT: Commercial lighting for ambient and display applications is mostly based on blue light-emitting diodes (LEDs) combined with phosphor materials that convert some of the blue light into green, yellow, orange, and red. Not many phosphor materials can offer stable output under high incident light intensities for thousands of operating hours. Even the most promising LED phosphors saturate in high-power applications, that is, they show decreased light output. The saturation behavior is often poorly understood. Here, we review three popular commercial LED phosphor materials, $Y_3Al_5O_{12}$ doped with Ce^{3+}, $CaAlSiN_3$ doped with Eu^{2+}, and K_2SiF_6 doped with Mn^{4+}, and unravel their saturation mechanisms. Experiments with square-wave-modulated laser excitation reveal the dynamics of absorption and decay of the luminescent centers. By modeling these dynamics and linking them to the saturation of the phosphor output intensity, we distinguish saturation by ground-state depletion, thermal quenching, and ionization of the centers. We discuss the implications of each of these processes for LED applications. Understanding the saturation mechanisms of popular LED phosphors could lead to strategies to improve their performance and efficiency or guide the development of new materials.

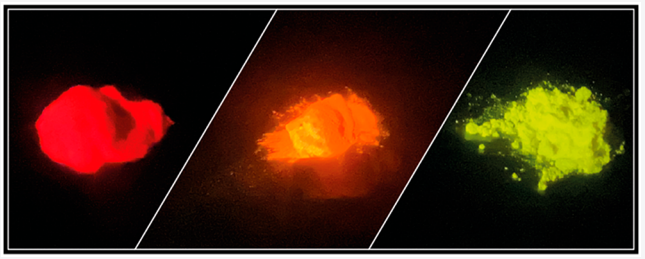

KEYWORDS: *phosphors, saturation, droop, LEDs, lanthanides, Mn^{4+} luminescence, spectroscopy*

Over the past few decades, light-emitting diodes (LEDs) have become mainstream for many lighting applications because of their high efficiency, low cost, small size, long device lifetimes, and other advantageous properties.[1−5] Since LEDs typically emit one saturated color, color conversion by downconverter materials is commonly used for applications that require white-light or multicolor emission. Over the past decades, only a few downconverter materials have emerged as viable for commercial LED applications, which can require operating lifetimes of over 50000 h at output intensities of up to 1 W mm^{-2}, while the temperatures of the phosphor material can reach up to 120 °C.[6−10] Commercially used LED phosphors are often inorganic crystals doped with lanthanide ions, which still outcompete rapidly developing alternatives like quantum dots and perovskites.[11−13] Especially yellow/green emitting Ce^{3+}-doped garnets, for example, $Y_3Al_5O_{12}:Ce^{3+}$ ("YAG:Ce^{3+}"), and red/infrared emitting Eu^{2+}-doped nitrides, for example, $CaAlSiN_3:Eu^{2+}$ ("CASN:Eu^{2+}"), have proven their value as LED phosphors over the past years.[6,7,14−16] These materials can be made with a close to 100% internal quantum yield and prolonged LED operating hours without severe degradation.[17−20]

Unfortunately, even the best performing phosphors suffer from thermal quenching at high temperatures and "droop" or "saturation quenching" at high light intensities. These unwanted effects are often already observed at LED operating conditions.[20,21,30,22−29] CASN:Eu^{2+}, for example, shows a decrease in light output of about 15% when used in high-power LEDs (incident intensity approximately 1 W mm^{-2}).[23] For applications operating at even higher powers, such as automotive head lights and projector devices (incident intensity up to 5−10 W mm^{-2}), the quenching issues become even more severe.[30,31] Despite rigorous optimization efforts mainly focused on controlling the phosphor temperature, only Ce-doped garnets (e.g., YAG:Ce^{3+}) are known to have acceptable performance in such high-power applications, while no red-emitting material is available.[22,25,30,32−37] These issues have until now limited the commercial success of phosphor-converted solid-state lighting for ultrahigh-power applications, despite impressive improvements in LED and device design.[38,39]

Mitigation of saturation and thermal-quenching effects is clearly important for applications, but the underlying physical mechanisms are still poorly understood. This makes it difficult to predict the applicability of promising new phosphors in terms of saturation behavior. For example, the development of

Received: March 11, 2021
Published: May 17, 2021

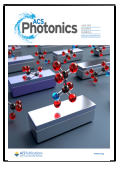

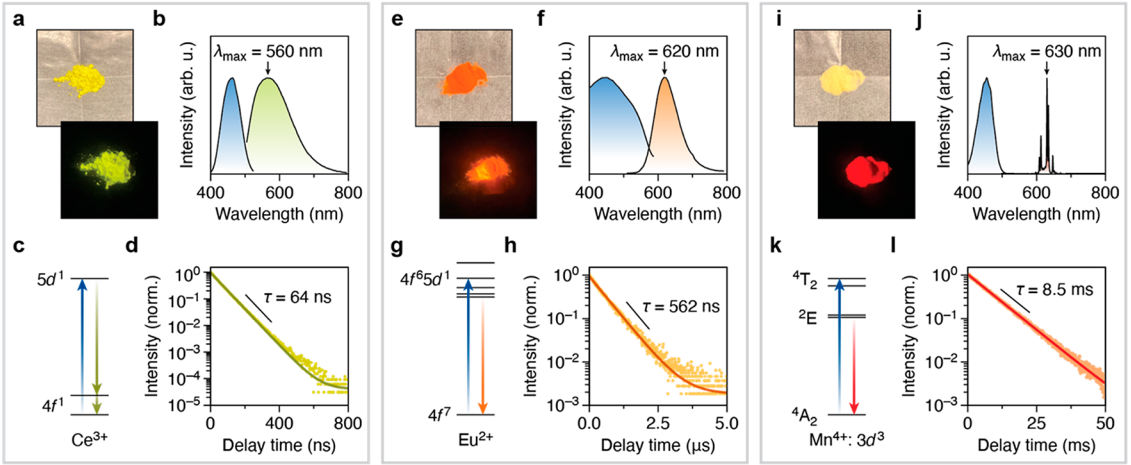

Figure 1. Characteristics of the three phosphor materials studied. (a) Real-color photographs of YAG:Ce^{3+} phosphor powder under ambient illumination (top) and its photoluminescence upon blue illumination (bottom). (b) Excitation (blue) and emission spectra of YAG:Ce^{3+}. (c) Energy level scheme of Ce^{3+} in YAG, with absorbing (upward arrow) and emitting (downward arrows) transitions indicated. (d) Photoluminescence decay curve of YAG:Ce^{3+} upon pulsed blue excitation. (e–h) Same as a–d, but for CASN:Eu^{2+}. (i–l) Same as a–d, but for KSF:Mn^{4+}.

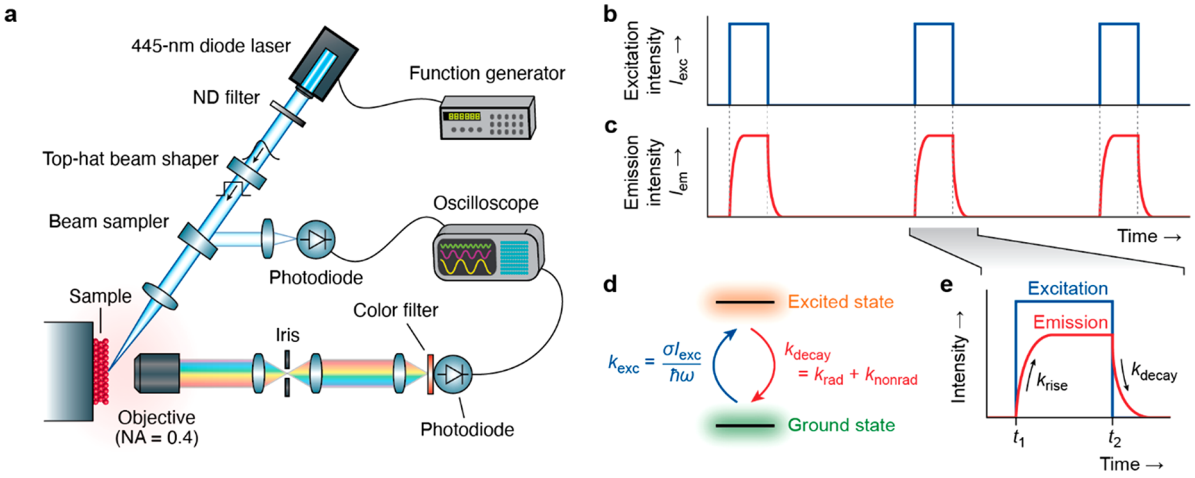

Figure 2. Modulated-intensity experiments. (a) Schematic of the experimental setup for measurements of luminescence dynamics with square-wave modulated excitation intensity. (b) Our excitation intensity profiles with square-wave modulation with tunable period, duty cycle, and maximum intensity. (c) The luminescence intensity of the phosphor follows excitation modulations with a delay. (d) Population dynamics in a two-level system with a ground state and an excited state. The rate constants for excitation and decay are k_{exc} and k_{decay}, respectively. (e) From the experimental luminescence intensity profile (depicted here schematically), we can extract k_{decay} and $k_{rise} = k_{exc} + k_{decay}$.

red-emitting phosphors with narrower emission bands than CASN:Eu^{2+} is an important challenge.[40] A well-known candidate is the line emitter K_2SiF_6:Mn^{4+} ("KSF:Mn^{4+}"), which has been extensively used in commercial displays where power densities are orders of magnitude lower than in high-power LEDs.[27,41−45] Although some KSF:Mn^{4+}-containing LED devices are on the market, it remains unclear to what extent the application potential of this phosphor is limited by its relatively poor saturation behavior.[42,46]

In this paper, we unravel the dominant saturation mechanisms for three of the most common phosphors used in commercial applications today: YAG:Ce^{3+}, CASN:Eu^{2+}, and KSF:Mn^{4+}. Emission measurements with square-wave-modulated excitation reveal simultaneously the emission intensities and dynamics of the phosphors. This allows us to identify a regime of "mild" conditions, with relatively low incident intensities and efficient heat dissipation, where the saturation behavior can be understood purely in terms of ground-state depletion. The threshold incident intensity, at which ground-state depletion becomes important, depends on the phosphor. As we heat the phosphors and increase the incident intensity further, other saturation mechanisms emerge, depending on the specific phosphor material. YAG:Ce^{3+} and KSF:Mn^{4+} suffer from thermal quenching, while CASN:Eu^{2+} shows signatures of thermal and photoionization, which also quench the luminescence. We conclude with a discussion of the implications of our results for the use of these phosphors in LEDs.

RESULTS

Figure 1 shows the basic properties of the three phosphor materials we investigated. YAG:Ce^{3+}, with 2.8% doping concentration, has a yellow appearance and shows green/yellow luminescence (Figure 1a). The broad emission band, peaking at 560 nm (Figure 1b), depending on the Ce^{3+} content, is due to the $5d \rightarrow 4f$ transition of Ce^{3+} (Figure 1c)

https://doi.org/10.1021/acsphotonics.1c00372
ACS Photonics 2021, 8, 1784−1793

with an excited-state lifetime of 64 ns (Figure 1d). The appearance and photoluminescence of CASN:Eu^{2+}, with 3.1% doping concentration, are both orange (Figure 1e). The emission peaks at 620 nm (Figure 1f) and originates from the $4f^6 5d^1 \rightarrow 4f^7$ transition of Eu^{2+} (Figure 1g) with an excited-state lifetime of 562 ns (Figure 1h). Finally, KSF:Mn^{4+}, with 2.1% doping concentration, looks pale yellow in reflection but shows strong deep red luminescence (Figure 1i). The sharp emission lines around 630 nm are phonon sidebands of the intraconfigurational $^2E \rightarrow {}^4A_2$ transition of Mn^{4+} ($3d^3$ configuration) in octahedral symmetry. The excited-state lifetime is as long as 8.5 ms.

To investigate the saturation behavior of the phosphors, we load them on the specialized setup built at Seaborough Research, schematically depicted in Figure 2a. The samples are illuminated with a 445 nm diode laser, producing an approximately homogeneous intensity profile at the location of the sample over an excitation spot of 90 × 90 μm^2 or 200 × 200 μm^2, depending on the experiment. The laser intensity is square-wave-modulated with a tunable period and duty cycle and the incident intensity level is tuned with a set of neutral density filters in the excitation path (Figure 2b). We correct the data for minor fluctuations of the laser intensity, which are recorded by a photodiode that samples a portion of the excitation beam. Luminescence from the illuminated area is collected by an objective, spatially selected with an iris, spectrally filtered, and sent to a photodiode.

The luminescence intensity does not follow the modulation of excitation intensity instantly, but instead responds with some delay (Figure 2c). This slow response provides important information about the dynamics of excitation and relaxation of the luminescent centers in the phosphor material. The simplest possible model for this treats the centers as two-level systems, with a ground state and an excited state (Figure 2d). The population dynamics for the excited state are described by the rate equation

$$\frac{dp}{dt} = k_{exc}[1 - p(t)] - k_{decay}p(t) \quad (1)$$

Here, $p(t)$ is the probability to find a center in the excited state at some moment in time t, k_{exc} is the rate constant for excitation, and k_{decay} is the rate constant for decay. The excitation rate $k_{exc} = \sigma I_{exc}/\hbar\omega$ depends on the absorption cross-section σ of a center, the excitation intensity I_{exc} (with SI units of W m^{-2}), and on the excitation photon energy $\hbar\omega$. The decay rate k_{decay} may be due to a combination of radiative and nonradiative decay pathways. Solving eq 1 yields exponential decay dynamics following t_2, when the excitation intensity is turned off (see Figure 2e):

$$p(t) = p(t_2)e^{-k_{decay}(t-t_2)} \quad (2)$$

for $t > t_2$. Following t_1, when the excitation intensity is turned on, the rise of the excited-state population is also exponential:

$$p(t) = p(t_2)[1 - e^{-k_{rise}(t-t_1)}] \quad (3)$$

for $t_1 < t < t_2$ and with $k_{rise} = k_{exc} + k_{decay}$. See Supporting Information, section S1 for a more extensive mathematical derivation. As the emission intensity from the sample is proportional to excited-state population, both k_{exc} and k_{decay} can be determined from a measurement of the luminescence dynamics with square-wave-modulated excitation.

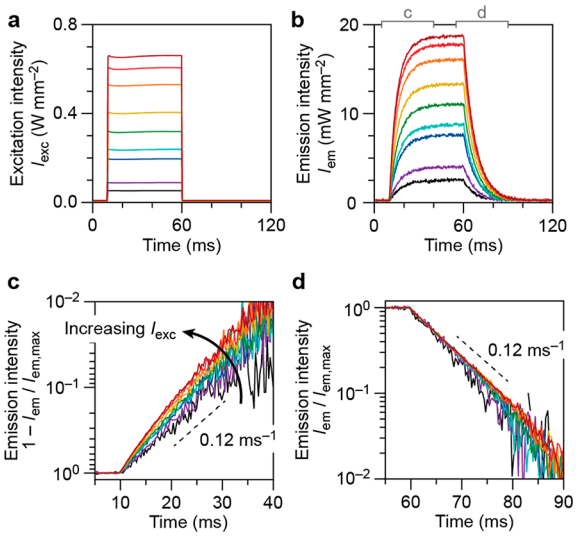

Figure 3. Rise and decay dynamics of KSF:Mn^{4+} under mild conditions. (a) Time dependence of the excitation intensity in nine different experiments on a thin layer of KSF:Mn^{4+}, with different peak excitation intensities as measured by the calibrated beam sampler in the excitation path (see Figure 2a). The total modulation period was 1 s with a 5% duty cycle. (b) Corresponding time dependence of the emission intensity. The colors of the different experiments match those in (a). (c) Zoom-in of the rise dynamics. The intensity axis is converted such that exponential rise produces a straight line. (d) Zoom-in of the decay dynamics on a logarithmic scale. The time ranges of the zoom-ins are indicated in (b). In all panels, the color coding indicates different peak intensities of I_{exc} = 0.05 (black), 0.09 (purple), 0.20 (blue), 0.23 (cyan), 0.21 (green), 0.40 (yellow), 0.53 (orange), 0.60 (red), and 0.66 (dark red) W mm^{-2}.

Figure 3 presents the results of a set of square-wave experiments on KSF:Mn^{4+}. We obtained a commercial sample by breaking open a commercial ZTE Nubia Z9 mini smartphone and extracting a few red-luminescing KSF:Mn^{4+} phosphor grains. For these measurements we used "mild" experimental conditions, meaning that (1) the grains were placed on an indium foil directly connected to a heat sink, (2) the peak excitation intensity was limited to a maximum of 0.7 W mm^{-2}, (3) the duty cycle was set to no more than 5% (Figure 3a), and (4) the heat sink was kept at room temperature. The luminescence intensity shows slow rise and decay over time scales of the Mn^{4+} excited-state lifetime of 8.5 ms (Figure 3b; compare with Figure 1l). Figure 3c and d show zoom-ins of the rise and decay dynamics. The decay dynamics are exponential with k_{decay} = 0.12 ms^{-1}, independent of excitation intensity (Figure 3d), matching the photoluminescence decay measurement with ns excitation in Figure 1l. We conclude that our 50 ms excitation pulses of up to 0.7 W mm^{-2} do not open nonradiative decay pathways. Excitation in the blue and the emission in the red (Figure 1j) inevitably leads to some heat generation, but the constant decay dynamics (Figure 3d) prove that under our mild conditions this is not sufficient to lead to thermal quenching. The rise dynamics are also exponential but accelerate with increasing excitation intensity (Figure 3c). This is expected, as $k_{rise} = k_{exc} + k_{decay}$ (eq 3). As k_{exc} is proportional to excitation intensity, the rise dynamics accelerate for stronger excitation. Figure S1 shows similar measurements and qualitatively similar results for CASN:Eu^{2+}, where we used an excitation modulation frequency of 100 Hz and duty cycle of 0.1%. For YAG:Ce^{3+}

https://doi.org/10.1021/acsphotonics.1c00372
ACS Photonics 2021, 8, 1784−1793

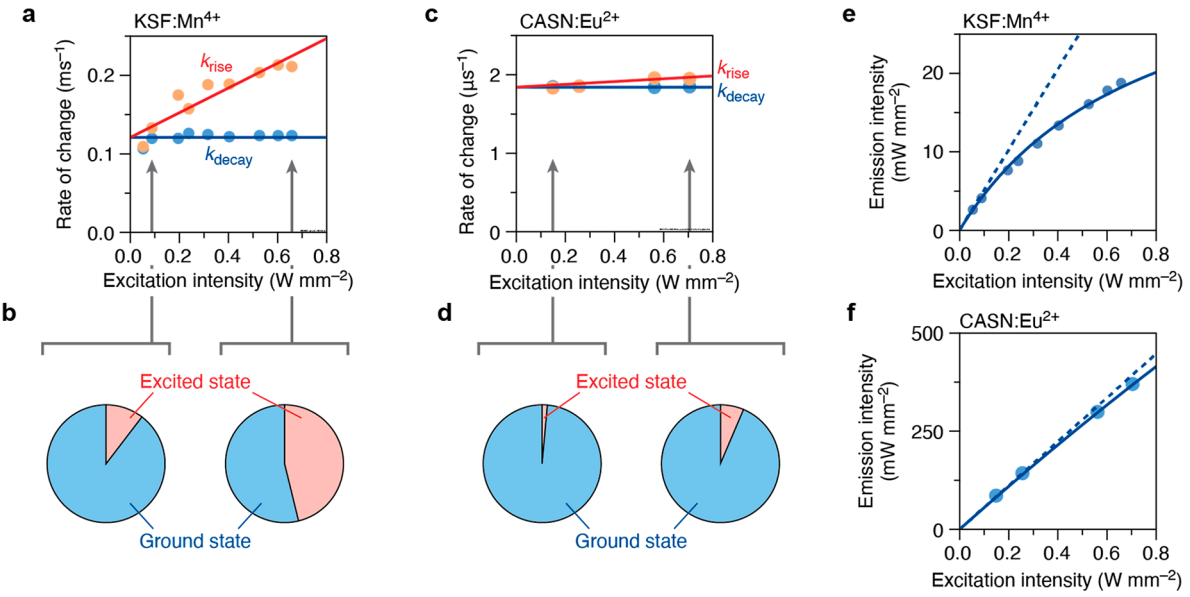

Figure 4. Rates of change of KSF:Mn^{4+} and CASN:Eu^{2+} reveal ground-state depletion. (a) Photoluminescence rise (red) and decay (blue) rates in a square-wave-pumped experiment on KSF:Mn^{4+} as a function of peak excitation intensity, as fitted from the data in Figure 3. (b) Pie charts of the calculated steady-state excited-state (red) and ground-state (blue) populations of Mn^{4+} at excitation intensities of 0.09 W mm^{-2} (left) and 0.66 W mm^{-2} (right). (c, d) Same as (a) and (b), but for CASN:Eu^{2+}. The steady-state populations are calculated for 0.15 W mm^{-2} (left) and 0.71 W mm^{-2} (right). The corresponding square-wave experimental data can be found in Figure S1. (e) Peak emission intensity as a function of peak excitation intensity for KSF:Mn^{4+}. Data points = experimental data; solid line = model based on ground-state depletion using the parameters extracted from (a). (f) Same as (e), but for CASN:Eu^{2+} using the parameters extracted from (c).

(Figure S2), it is not possible to measure any clear dependence of dynamics on excitation intensity as the dynamics are too fast compared to the turn-on and turn-off response of the excitation laser (300 and 40 ns, respectively; Figure S2c). Nevertheless, for the sake of completeness, we present the dynamics data for YAG:Ce^{3+} in the Supporting Information, Figure S2. The CASN:Eu^{2+} and YAG:Ce^{3+} measurements were done on the same samples, as presented in Figure 1.

Figure 4a presents k_{rise} and k_{decay} as a function of I_{exc}, as obtained by fitting exponential dynamics to the data of Figure 3 on KSF:Mn^{4+}. A model of constant k_{decay} (blue line) and linearly increasing $k_{rise} = k_{decay} + k_{exc}$ (red line) matches the fit results well. The observation of these simple trends confirms that slight but inevitable heating has no effect on the phosphor dynamics under mild conditions. We see that k_{rise} exceeds k_{decay} by up to 80%, meaning that, on the range of I_{exc} considered here, the excitation rate of Mn^{4+} is comparable to the emission rate. This will create a significant steady-state population of the Mn^{4+} ^2E excited state and, consequently, depletion of the ground state. To calculate this quantitively, we extract the absorption cross-section $\sigma_{eff} = 7 \times 10^{-19}$ cm^2 of Mn^{4+} in microcrystalline KSF at 445 nm from the slope of the red line in Figure 4a. This value represents an "effective" absorption cross-section, affected by scattering of excitation light in the phosphor layer and reflection on the substrate which can enhance the electromagnetic field strength experienced by Mn^{4+}.[47] Indeed, σ_{eff} is an order of magnitude higher than the absorption cross sections of $\sigma = 0.3-1.7 \times 10^{-19}$ cm^2 measured for the same $^4A_2 \rightarrow {}^4T_2$ absorption transition in the isoelectronic luminescent center Cr^{3+} in various crystals.[48−50] Using the simple two-level model of Figure 2d, we can estimate the steady-state excited-state population

$$p_{ss} = \frac{\sigma_{eff} I_{exc}/h\omega}{\sigma_{eff} I_{exc}/h\omega + k_{decay}} \quad (4)$$

where subscript "ss" denotes "steady-state". The pie charts of Figure 4b show the calculated steady-state populations for two values of I_{exc} we used in the experiment. These steady-state populations are reached within a few tens of ms after excitation is turned on, as observed in Figure 3b.

Figure 4c shows k_{rise} and k_{decay} for CASN:Eu^{2+}, over the same range of I_{exc} as we studied for KSF:Mn^{4+}. Again, k_{decay} is constant, while k_{rise} increases linearly. This proves that, similar to KSF:Mn^{4+}, slight heating of CASN:Eu^{2+} under mild conditions does not affect the absorption and emission dynamics. However, k_{rise} is now only 7% faster than k_{decay} even at the highest I_{exc}. Clearly, for CASN:Eu^{2+} the excitation rate remains significantly slower than the emission rate, leading to less ground-state depletion than in KSF:Mn^{4+}. To illustrate this, in Figure 4d we show pie charts for CASN:Eu^{2+}, calculated with an absorption cross-section $\sigma_{eff} = 6 \times 10^{-16}$ cm^2 (from the fit in Figure 4c). Indeed, the steady-state excited-state populations are much lower than for KSF:Mn^{4+} (compare Figure 4b). As for KSF:Mn^{4+} (Figure 4a,b), our value of σ_{eff} for CASN:Eu^{2+} is significantly larger than the absorption cross-section measured of $\sigma \approx 10^{-17}$ cm^2 for Eu^{2+} in transparent media,[51,52] most likely because of scattering in the phosphor film and reflection on the substrate. Similar analysis for YAG:Ce^{3+} suffers from uncertainties because the excited-state lifetime is too short compared to the modulation response time of our excitation laser (Figure S2).

Figure 4e,f show the saturation characteristics of our KSF:Mn^{4+} and CASN:Eu^{2+} phosphors: the emitted intensity I_{em} (under steady-state conditions, *e.g.* at t = 50−60 ms in Figure 2b for KSF:Mn^{4+}) as a function of I_{exc}. The observation of significant saturation of KSF:Mn^{4+} at excitation intensities lower than I_{exc} 0.2 W mm^{-2} is in line with earlier studies.[42,53]

https://doi.org/10.1021/acsphotonics.1c00372
ACS Photonics 2021, 8, 1784−1793

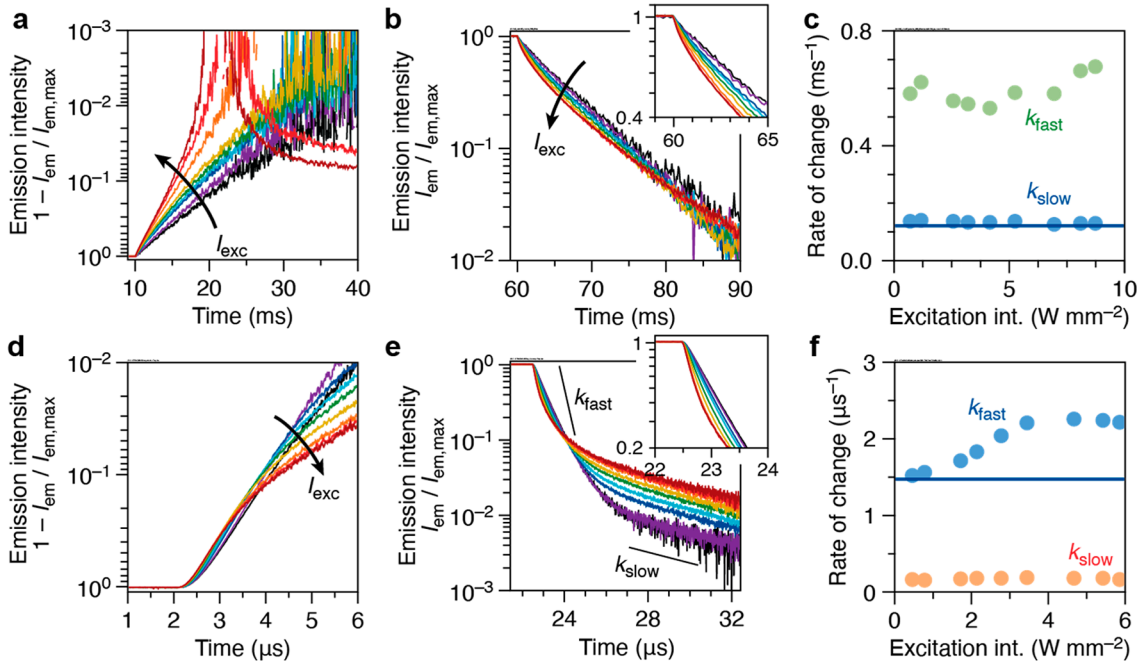

Figure 5. Photoluminescence from KSF:Mn^{4+} and CASN:Eu^{2+} under harsh conditions and strong excitation. (a) The rise dynamics of photoluminescence from KSF:Mn^{4+} under harsh conditions of external heating and excitation with high duty cycle at increasing peak excitation intensity I_{exc}. The different colors indicate I_{exc} = 0.7 (black), 1.2 (purple), 2.5 (blue), 3.2 (cyan), 4.2 (green), 5.2 (yellow), 6.9 (orange), 8.1 (red), and 8.7 (dark red) W mm^{-2}. At the highest I_{exc}, the emission intensity peaks at approximately t = 20 ms, which is 10 ms after the excitation is turned on, and then decreases by ∼10%. Note the scale on the y-axis: 10% intensity decrease from the maximum corresponds to $1 - I_{em}/I_{em,max} = 10^{-1}$. (b) The corresponding decay dynamics. The inset is a zoom-in of the fast decay component. (c) Rate constants from a biexponential fit to the decay dynamics of (b) as a function of excitation intensity. The blue line represents the excitation-independent decay dynamics under mild conditions (same as in Figure 4a). (d–f) Same as a–c, but for CASN:Eu^{2+}. For CASN:Eu^{2+} we used excitation intensities of I_{exc} = 0.5 (black), 0.8 (purple), 1.7 (blue), 2.1 (cyan), 2.8 (green), 3.5 (yellow), 4.7 (orange), 5.4 (red), and 5.9 (dark red) W mm^{-2}.

The solid lines are fits to a model of saturation due to ground-state depletion, using that I_{em} is proportional to the steady-state excited-state population p_{ss} (eq 4). We fix k_{decay} and σ_{eff} in the fits, and optimize only the proportionality constant between p_{ss} and I_{em}. By comparing with a hypothetical scenario without ground-state depletion (dashed lines; $I_{em} \propto \sigma_{eff} I_{exc}/k_{decay}\hbar\omega$), we see, again, that KSF:Mn^{4+} saturates significantly more strongly than CASN:Eu^{2+}. With a single set of values for the excitation and decay rates, the model captures both experimental saturation behavior (Figure 4e,f) and the dynamics (Figure 4a,c). Clearly, under the mild conditions of these experiments and up to I_{exc} = 0.8 W mm^2, ground-state depletion is the dominant reason for photoluminescence saturation of these phosphors, as previously concluded by Sijbom et al. for KSF:Mn^{4+},[43] and Shchekin et al. for CASN:Eu^{2+}.[23]

Next, we subject the phosphors to harsher conditions. We vary the excitation intensity over a wider range of up to several W mm^{-2}. For CASN:Eu^{2+}, we additionally heat the phosphor to 120 °C by increasing the temperature of the heatsink connected to the indium foil and increase the duty cycle of the square-wave-modulated excitation laser to 99.8% at a modulation period of 10 ms. Figure 5 shows the results of these experiments for KSF:Mn^{4+} and CASN:Eu^{2+}. Figure S2 shows our data on YAG:Ce^{3+}.

Figure 5a–c present the emission and excitation dynamics of KSF:Mn^{4+} under harsh experimental conditions. The rise dynamics (Figure 5a) keep accelerating up to I_{exc} = 8.7 W mm^{-2}, qualitatively consistent with our understanding that $k_{rise} = k_{decay} + k_{exc}$. However, at the highest I_{exc} > 6 W mm^{-2} (orange and red lines), the emitted intensity peaks at ∼10 ms after excitation is turned on and then decreases by a few percent over the next 10 ms. The decay dynamics (Figure 5b) also show new features compared to the experiments under mild conditions (Figure 3d): in addition to an excitation-independent decay component with a rate constant of $k_{slow} = k_{decay}$ = 1/(7.5 ms), a fast component k_{fast} appears. The amplitude of the fast component grows with increasing I_{exc}, while the rate constant is approximately constant at 0.6 ms^{-1} (Figure 5c).

The observations of Figure 5a–c no longer follow the simple trends of eqs 2,3 and, instead, are consistent with excitation-induced heating of the KSF:Mn^{4+} phosphor film. The decay rate of the Mn^{4+} ^2E excited state in KSF,[54] as well as in other hosts such as K_2TiF_6,[55] accelerates with increasing temperature. More precisely, radiative decay is phonon-assisted and its rate k_{rad} increases from 0.12 ms^{-1} at room temperature to 0.19 ms^{-1} at T = 200 °C, while nonradiative decay due to thermally activated crossover to the Mn^{4+} $^4T_2$ state sets in above T > 200 °C.[54,55] While we do not measure the temperature directly, the observation of a drop in emission intensity 10–20 ms after illumination turn-on (Figure 5a) implies that we reach the latter regime of thermal quenching, that is, the local temperature T > 200 °C for our highest excitation intensities I_{exc} > 6 W mm^{-2}. The few-ms time scales of the emission drop after initial rise (Figure 5a) and the fast component in the decay dynamics (Figure 5b) reflect a finite temperature equilibration time after illumination is modulated. Figure S2 shows indications of heat-induced quenching for YAG:Ce^{3+} as well, causing an intensity roll-off at I_{exc} > 2.5 W

https://doi.org/10.1021/acsphotonics.1c00372
ACS Photonics 2021, 8, 1784–1793

mm^{-2}. This indicates that we reach temperatures in excess of 150 °C in YAG with 2.8% Ce^{3+}.[22]

The behavior of CASN:Eu^{2+} under harsh conditions is markedly different from that of KSF:Mn^{4+} but also clearly deviate from the predictions of the simple rate-equation model (eqs 2 and 3). Both the rise and decay dynamics become close to biexponential (Figures 5d,e). In contrast to KSF:Mn^{4+}, the fast component matches the measurements under mild conditions (Figure 5f; compare with Figure 4c), while a second component with a temperature-independent rate constant of k_{slow} = 0.17 μs^{-1} grows in amplitude with increasing I_{exc}. This behavior can be explained by ionization of Eu^{2+}, which produces slow afterglow luminescence. In this process, Eu^{2+} ejects the *d*-electron from its $4f^65d^1$ excited state to the conduction band of the CASN host material, resulting in a somewhat faster initial decay (k_{fast} in Figure 5f) than under mild conditions. The electron is temporarily trapped in a shallow trap before it recombines with the Eu^{3+} $4f^6$ core and recreates the $4f^65d^1$ excited state. This sequence of events effectively increases the lifetime of the excited state, leading to afterglow luminescence (Figure 5e) and slower equilibration after the excitation light is turned on (Figure 5d). It is difficult to integrate and quantify the contribution of afterglow luminescence precisely, as the dynamics are multiexponential and slow compared to the period of our excitation modulation. As k_{fast} (Figure 5f) under harsh conditions is faster than k_{decay} = 1.5 μs^{-1} under mild conditions (Figure 4c), we know that the ionization process continues after the excitation laser turns off. Ionization is thus at least in part thermal, which has also been observed by Ueda et al.[26] Nevertheless, photoionization by excited state absorption may play a role as well.[27]

Figure 6a shows the saturation characteristics we measured on KSF:Mn^{4+}. Although the first signatures of saturation set in at mild excitation of I_{exc} = 0.2 W mm^{-2} (Figure 4e), I_{em} continues to increase until at least I_{exc} = 10 W mm^{-2} (Figure 6a). These observations are consistent with the results reported by Sijbom et al.[43] Significantly stronger saturation would be expected based on the values of k_{rad} and σ_{eff} extracted from experiments under mild conditions (red solid line in Figure 6a). This relatively weak saturation of KSF:Mn^{4+} under strong excitation is likely a surprising benefit of heating. The steady-state emission intensity I_{em} is proportional to k_{rad} and, as we wrote above, k_{rad} increases with increasing temperature.[54,55] This affects the saturation behavior, as realized previously by Sijbom et al.[43] Incorporating this effect in our model for saturation (eq 4) and assuming that laser-induced heating scales linearly with I_{exc} produces a closer match (blue line in Figure 6a) to the experimental data than the bare model but still underestimates I_{em}. Possibly, the continued increase of I_{em} is further caused by an artifact of our measurement with a focused laser on a microcrystalline grain. As the Mn^{4+} ions in the center of the spot saturates, the excitation light is scattered further into the grains. Consequently, the effective sample volume probed increases with I_{exc} (Figure S4), hiding the full extent of the saturation effect we would otherwise observe.

For our measurements on CASN:Eu^{2+} we can also construct a quantitative model of the saturation under harsh conditions. The emission intensity saturates more strongly than we expect based on the ground-state depletion model that worked so well for mild conditions (Figure 6b; compare data with red line). From the dynamics (Figure 5d–f), we concluded that this is due to ionization of Eu^{2+} from the $4f^65d^1$ excited state. We construct a simple rate-equation model of this process (Figure 6c). We assume a single ionization rate k_{ion} from the $(Eu^{2+})^*$ excited state, the value of which we set at $k_{ion} = k_{fast} - k_{decay}$, where k_{fast} is the excitation-dependent fast decay component of the experiments under harsh conditions (Figure 5f) and k_{decay} is the excitation-independent decay rate of the experiments under mild conditions (Figure 4c). For the recombination rate k_{rec}, we take the slow decay component k_{slow} (Figure 5f). With this treatment we neglect photoionization and a potential distribution of trap states leading to a distribution of recombination rates. We nevertheless see that our simplified afterglow model (blue line in Figure 6b) captures the saturation characteristics of CASN:Eu^{2+} reasonably well. Based on this model, we estimate that the steady-state population of ionized Eu^{3+} is more than 50% at I_{exc} > 4 W mm^{-2} (Figure 6d). This explains the poor performance of CASN:Eu^{2+} under strong excitation. The drop of intensity at the highest excitation intensities, which is not reproduced by our model, is likely due to photoionization. Qualitatively, our analysis thus indicates that both thermal and photoionization are significant under harsh conditions.

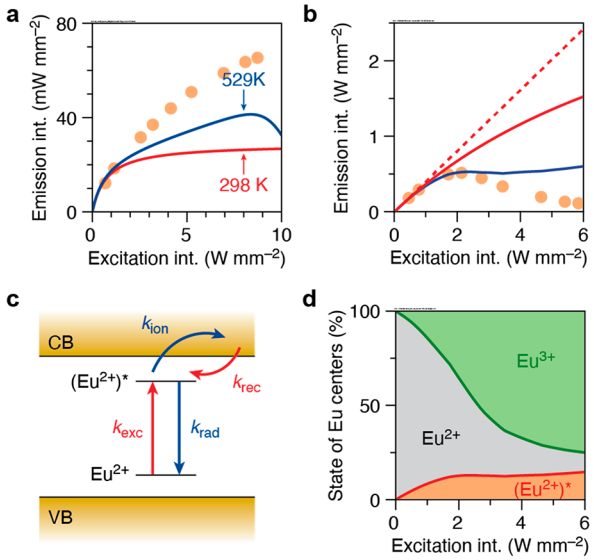

Figure 6. Saturation of phosphors under strong excitation and external heating. (a) Saturation characteristics of our KSF:Mn^{4+} measurement under harsh conditions. The red line depicts ground-state depletion model using the parameters from Figure 4e. The blue line is a model of ground-state depletion, assuming excitation-induced heating and accounting for the temperature-dependent radiative decay rate of KSF:Mn^{4+} (see Figure S3 for more details).[54] (b) Same, but for CASN:Eu^{2+}. The blue line shows the result of the afterglow model. The red dashed line is the scenario without ground-state depletion. (c) Schematic of the afterglow model, depicting ionization (k_{ion}) of the $(Eu^{2+})^*$ excited state and return (k_{rec}) of the conduction-band (CB) electron. (d) Steady-state populations of the Eu^{2+} ground state (gray), $(Eu^{2+})^*$ excited state (red), and Eu^{3+} ionized state (green), calculated with the afterglow model.

DISCUSSION

In Figure 7 we consider the implications of our findings for phosphor-converted LED lighting. Figure 7a summarizes our findings on ground-state depletion for the three phosphors studied. The onset of ground-state depletion is defined by the effective absorption cross-section σ_{eff} of the active ions at the LED excitation wavelength (450 nm) and their decay rate k_{decay}. We define I_{10} as the excitation intensity at which the

https://doi.org/10.1021/acsphotonics.1c00372
ACS Photonics 2021, 8, 1784–1793

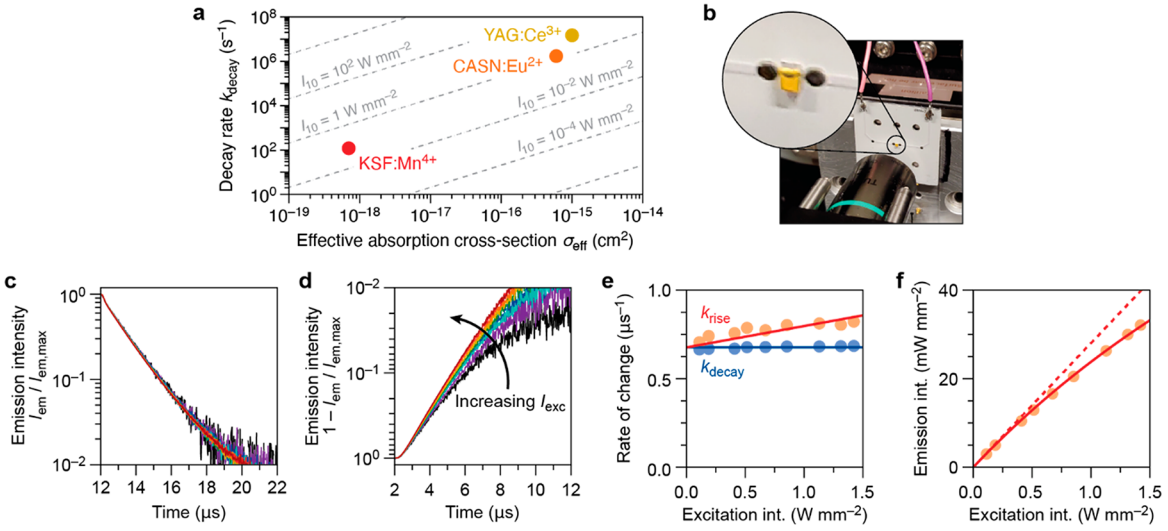

Figure 7. Implications for LED applications. (a) Overview of the (low-power) decay rates k_{decay} and the effective absorption cross-section σ_{eff} (at 455 nm) of the three phosphors we studied. Note that σ_{eff} of CASN:Eu^{2+} and KSF:Mn^{4+} are determined from the rise dynamics (Figure 4a,c), while for YAG:Ce^{3+} we could only use the saturation characteristics (Figure S2f) because the phosphor dynamics are too fast compared to the turn-on and turn-off rates of our setup for quantitative measurements. The gray dashed lines are contours for different values of excitation intensity I_{10} at which 10% of the active ions are in their excited state in the steady state (eq 5). (b) Photograph of our setup to measure the saturation dynamics of the CASN:Eu^{2+} phosphor inside a commercial white LED device. (c) Decay dynamics and (d) rise dynamics of CASN:Eu^{2+} measured in the setup of (b), at increasing square-wave-modulated (duty cycle 0.1%) excitation intensity with an external laser with peak intensities of I_{exc} = 0.1 (black), 0.2 (purple), 0.4 (blue), 0.5 (cyan), 0.7 (green), 0.9 (yellow), 1.1 (orange), 1.3 (red), and 1.4 (dark red) W mm^{-2}. (e) The rates of decay (blue) and rise (red) determined by fitting the data of (c) and (d), respectively. (f) The saturation characteristics of CASN:Eu^{2+} fitted to the model of ground-state depletion (red solid line; eq 4) using k_{decay} and σ_{eff} determined from the data of (e). The dashed red line is the hypothetical case without ground-state depletion.

dynamic equilibrium between absorption and emission (Figure 2d) creates a steady-state excited-state population of 10%:

$$I_{10} = \frac{k_{decay}\hbar\omega}{9\sigma_{eff}} \quad (5)$$

where $\hbar\omega$ is the photon energy of the excitation light. I_{10} is the approximate threshold excitation intensity at which ground-state depletion sets in. More precisely, at I_{10} the emission intensity is decreased by 10% compared to what it would be without saturation. The gray lines in Figure 7a are iso-contours of I_{10}. This plot places the three phosphors in the perspective of relevant LED incident intensities. Our estimate of σ_{eff} for YAG:Ce^{3+} (based on only the saturation characteristics; Figure S2) yields I_{10} = 7.5 W mm^{-2}, so ground-state depletion is a potential issue only for ultrahigh-power LED applications (>5 W mm^{-2}). This is supported by publications describing only minor saturation effects up to 10 W mm^{-2}, while saturation at even higher intensities was previously attributed to excited state absorption (ESA).[21,56,57] CASN:Eu^{2+} has I_{10} = 1.4 W mm^{-2} so the first effects of ground-state depletion become apparent for high-power LEDs (1 W mm^{-2}). Also, this conclusion is in line with the previously found onset of saturation for CASN:Eu^{2+}.[23] The threshold for KSF:Mn^{4+} lies more than an order of magnitude lower (I_{10} = 0.1 W mm^{-2}), explaining the known sensitivity of this material to saturation.[42,43] Note that the threshold for saturation by ground-state depletion I_{10} depends on the ratio of k_{decay} and σ_{eff}, rather than on k_{decay} alone.[42,43] In the case of KSF:Mn^{4+} excitation is in the spin-allowed $^4A_2 \rightarrow {}^4T_2$ absorption band while emission is due to the spin-forbidden $^2E \rightarrow {}^4A_2$ transition, which has a 3 orders of magnitude lower transition probability. It is this combination of relatively strong absorption and strongly forbidden emission that is responsible for the very low threshold for saturation and in fact was instrumental in the realization of population inversion in the first laser using the iso-electronic Cr^{3+} ion in ruby.[58] If the absorption of Mn^{4+} in KSF were weaker, it would not suffer from ground-state depletion at this low value of I_{10} despite the very long excited-state lifetime.

The radiative decay rate k_{decay} and absorption σ_{eff} are material properties but can to some extent be controlled by changing the environment. For example, an attractive strategy to increase the threshold for ground-state depletion could be to accelerate k_{decay} with photonic or plasmonic structures.[59,60] At the same time, such plasmonic or photonic structures would affect σ_{eff}, a concept that is used for photovoltaics and other applications.[61] Indeed, we extract relatively large values for σ_{eff} of our luminescent centers, which is likely a result of strong light scattering in our phosphor films increasing the excitation energy density experienced by the center.[47] Preventing scattering, for example by embedding phosphor grains in an index-matched resin, could potentially reduce σ_{eff} and thereby the threshold for ground-state depletion. However, index matching may be a challenging task for phosphors with a high index like CASN.[62] In addition, reducing σ_{eff} might be undesired since it would require more material or a higher doping level to achieve the same amount of absorption.

How do the saturation mechanisms we identified affect the performance of phosphors in LEDs? All three phosphors show ground-state depletion, although at different excitation thresholds (Figure 7a). The three phosphors studied react differently to the harsher conditions we imposed (Figures 5 and S2). YAG:Ce^{3+} and KSF:Mn^{4+} show signatures of thermal quenching at excitation intensities of I_{exc} > 5 W mm^{-2}, while CASN:Eu^{2+} suffers from quenching by thermal and photoionization at I_{exc} > 1 W mm^{-2}. All saturation mechanisms

https://doi.org/10.1021/acsphotonics.1c00372
ACS Photonics 2021, 8, 1784−1793

reduce the phosphor emission and thereby shift the color output of phosphor-converted LED lighting. Ground-state depletion reduces phosphor absorption and thereby the external quantum yield (i.e., emitted intensity divided by input intensity), but not the internal quantum yield (i.e., emitted intensity divided by absorbed intensity). Ground-state depletion is thus a lossless saturation mechanism, which can be compensated with a higher phosphor loading on the LED or could even be put to use for color tuning. Thermal quenching, as in YAG:Ce^{3+} and KSF:Mn^{4+}, introduces a nonradiative decay pathway, thereby reducing both the external and the internal quantum yield. Photo- and thermal ionization, as in CASN:Eu^{2+}, strongly depletes the ground-state population of optical centers (Figure 6d), so it reduces absorption and thereby the external quantum yield. As long as the ejected charge carriers return and eventually produce emission (as in our model of Figure 6c), the internal quantum yield is not affected. It is, however, well-known that thermal ionization often leads to quenching due to nonradiative recombination of charge carriers at quenching sites. Both thermal ionization and ionization by excited-state absorption may contribute to the drop in emission intensity from YAG:Ce^{3+} under strong illumination (Figure S2).[21,56,57]

With the setup of Figure 7b, we characterize the saturation mechanisms at play in a real LED. We place a commercial LED module (Lumileds Luxeon Z 3000 K LED) in our optical setup and excite the phosphor layer with our square-wave-modulated laser (duty cycle D = 0.1%, no external heating) with increasing peak excitation intensity up to I_{exc} = 1.4 W mm^{-2}. The phosphor layer constitutes a combination of YAG:Ce^{3+} and CASN:Eu^{2+}. A 680 nm long-pass filter selects (primarily) the Eu^{2+} emission. We observe I_{exc}-independent decay dynamics (Figure 7c), showing that we are not yet in the regime of ionization (in contrast to Figure 5e). The rise dynamics, on the other hand, accelerate with increasing I_{exc} (Figure 7d). This is a signature of ground-state depletion, as in Figure 4. The I_{exc}-independent decay rate k_{decay} = 0.68 μs^{-1} is somewhat slower while the effective absorption-cross section σ_{eff} = 5 × 10^{-16} cm^2 is slightly smaller than for our measurement on the phosphor film (compare Figures 7e to Figure 4). These differences are likely due to the resin embedding of the phosphor grains in the LED, which affects the density of optical states[60] and the scattering. Using these parameters, we can reproduce the saturation characteristics of the LED phosphor layer (Figure 7f). The saturation behavior of CASN:Eu^{2+} and its underlying causes is thus the same in an LED geometry as in our measurements on a phosphor film.

To summarize, we were able to identify the dominant saturation mechanisms in common LED phosphors with time-resolved emission measurements under square-wave-modulated excitation. With our quantitative model, we extracted the sensitivity to and threshold for ground-state depletion from the rise and decay dynamics of the emitted intensity in response to modulations of the excitation light. Under harsher conditions (e.g., stronger and longer photoexcitation and external heating), YAG:Ce^{3+} and KSF:Mn^{4+} showed thermal quenching, while CASN:Eu^{2+} showed ionization and afterglow luminescence. We discussed how each of these saturation mechanisms is relevant in phosphor-converted LEDs.

■ ASSOCIATED CONTENT

Supporting Information

The Supporting Information is available free of charge at https://pubs.acs.org/doi/10.1021/acsphotonics.1c00372.

Additional data on CASN:Eu^{2+} and YAG:Ce^{3+} under square-wave excitation; modeling of heating effects on KSF:Mn^{4+} saturation; images of the phosphor luminescence; derivation of the rise and decay dynamics (PDF)

■ AUTHOR INFORMATION

Corresponding Authors

Marie Anne van de Haar − *Seaborough Research BV, Matrix VII Innovation Center, 1098 XG Amsterdam, The Netherlands;* orcid.org/0000-0003-2581-6076; Email: m.vandehaar@seaborough.com

Freddy T. Rabouw − *Utrecht University, 3584 CC Utrecht, The Netherlands;* orcid.org/0000-0002-4775-0859; Email: f.t.rabouw@uu.nl

Authors

Mohamed Tachikirt − *Seaborough Research BV, Matrix VII Innovation Center, 1098 XG Amsterdam, The Netherlands*

Anne C. Berends − *Seaborough Research BV, Matrix VII Innovation Center, 1098 XG Amsterdam, The Netherlands;* orcid.org/0000-0003-4249-2843

Michael R. Krames − *Seaborough Research BV, Matrix VII Innovation Center, 1098 XG Amsterdam, The Netherlands; Arkesso LLC, Palo Alto, California 94306, United States*

Andries Meijerink − *Utrecht University, 3584 CC Utrecht, The Netherlands;* orcid.org/0000-0003-3573-9289

Complete contact information is available at: https://pubs.acs.org/10.1021/acsphotonics.1c00372

Notes

The authors declare no competing financial interest.

■ ACKNOWLEDGMENTS

This work is part of the research program Innovation Fund Chemistry (LIFT) with Project 731.017.401, which is (partly) financed by the Dutch Research Council (NWO). F.T.R. is supported by NWO Veni Grant 722.017.002 and by The Netherlands Center for Multiscale Catalytic Energy Conversion (MCEC), an NWO Gravitation program funded by the Ministry of Education, Culture and Science of the Government of The Netherlands.

■ REFERENCES

(1) Krames, M. R.; et al. Status and future of high-power light-emitting diodes for solid-state lighting. *J. Disp. Technol.* **2007**, *3*, 160−175.

(2) Dupuis, R. D.; Krames, M. R. History, Development, and Applications of High-Brightness Visible Light-Emitting Diodes. *J. Lightwave Technol.* **2008**, *26*, 1154−1171.

(3) Steigerwald, D. A.; et al. Illumination with solid state lighting technology. *IEEE J. Sel. Top. Quantum Electron.* **2002**, *8*, 310−320.

(4) Chang, M. H.; Das, D.; Varde, P. V.; Pecht, M. Light emitting diodes reliability review. *Microelectron. Reliab.* **2012**, *52*, 762−782.

(5) Trivellin, N.; et al. A review on the reliability of GaN-based laser diodes. *IEEE Int. Reliab. Phys. Symp. Proc.* **2010**, *8*, 1−6.

(6) McKittrick, J.; Shea-Rohwer, L. E. Review: Down conversion materials for solid-state lighting. *J. Am. Ceram. Soc.* **2014**, *97*, 1327−1352.

(7) Setlur, A. A. Phosphors for LED-based solid-state lighting. *Electrochem. Soc. Interface* **2009**, *18*, 32−36.
(8) George, N. C.; Denault, K. A.; Seshadri, R. Phosphors for Solid-State White Lighting. *Annu. Rev. Mater. Res.* **2013**, *43*, 481−501.
(9) Huang, X. Red phosphor converts white LEDs. *Nat. Photonics* **2014**, *8*, 748−749.
(10) Cich, M. J.; et al. Bulk GaN based violet light-emitting diodes with high efficiency at very high current density. *Appl. Phys. Lett.* **2012**, *101*, 223509.
(11) Shirasaki, Y.; Supran, G. J.; Bawendi, M. G.; Bulović, V. Emergence of colloidal quantum-dot light-emitting technologies. *Nat. Photonics* **2013**, *7*, 13−23.
(12) Guner, T.; et al. A Review on Halide Perovskites as Color Conversion Layers in White Light Emitting Diode Applications. *Phys. Status Solidi A* **2018**, *215*, 1800120.
(13) Wei, Y.; Cheng, Z.; Lin, J. An overview on enhancing the stability of lead halide perovskite quantum dots and their applications in phosphor-converted LEDs. *Chem. Soc. Rev.* **2019**, *48*, 310−350.
(14) Uheda, K.; Hirosaki, N.; Yamamoto, H. Host lattice materials in the system Ca_3N_2-AlN-Si_3N_4 for white light emitting diode. *Phys. Status Solidi A* **2006**, *203*, 2712−2717.
(15) Uheda, K.; Hirosaki, N.; Yamamoto, Y.; Naito, A.; Nakajima, T.; Yamamoto, H. Luminescence properties of a red phosphor, $CaAlSiN_3$:Eu^{2+}, for white light-emitting diodes. *Electrochem. Solid-State Lett.* **2006**, *9*, 22−25.
(16) Ye, S.; Xiao, F.; Pan, Y. X.; Ma, Y. Y.; Zhang, Q. Y. Phosphors in phosphor-converted white light-emitting diodes: Recent advances in materials, techniques and properties. *Mater. Sci. Eng., R* **2010**, *71*, 1−34.
(17) Tsai, C. C.; et al. Investigation of Ce:YAG doping effect on thermal Aging for high-power phosphor-converted white-light-emitting diodes. *IEEE Trans. Device Mater. Reliab.* **2009**, *9*, 367−371.
(18) Oishi, M.; et al. High temperature degradation mechanism of a red phosphor, $CaAlSiN_3$:Eu for solid-state lighting. *J. Appl. Phys.* **2017**, *122*, 113104.
(19) Hu, Y.; et al. High temperature stability of Eu^{2+}-activated nitride red phosphors. *J. Rare Earths* **2014**, *32*, 12−16.
(20) Jang, M. S.; Choi, Y. H.; Wu, S.; Lim, T. G.; Yoo, J. S. Material properties of the Ce^{3+}-doped garnet phosphor for a white LED application. *J. Inf. Disp.* **2016**, *17*, 117−123.
(21) Lenef, A.; Raukas, M.; Wang, J.; Li, C. Phosphor Performance under High Intensity Excitation by InGaN Laser Diodes. *ECS J. Solid State Sci. Technol.* **2020**, *9*, 016019.
(22) Bachmann, V.; Ronda, C.; Meijerink, A. Temperature quenching of yellow Ce^{3+} luminescence in YAG:Ce. *Chem. Mater.* **2009**, *21*, 2077−2084.
(23) Shchekin, O. B.; et al. Excitation dependent quenching of luminescence in LED phosphors. *Phys. Status Solidi RRL* **2016**, *10*, 310−314.
(24) Setlur, A. A.; Shiang, J. J.; Hannah, M. E.; Happek, U. Phosphor quenching in LED packages: measurements, mechanisms, and paths forward. *Ninth International Conference on Solid State Lighting*; SPIE, 2009; Vol. *7422*, pp 74−81.
(25) Krasnoshchoka, A.; et al. Investigation of Saturation Effects in Ceramic Phosphors for Laser Lighting. *Materials* **2017**, *10*, 1407.
(26) Ueda, J.; Tanabe, S.; Takahashi, K.; Takeda, T.; Hirosaki, N. Thermal Quenching Mechanism of $CaAlSiN_3$:Eu^{2+} Red Phosphor. *Bull. Chem. Soc. Jpn.* **2018**, *91*, 173−177.
(27) Jansen, T.; Böhnisch, D.; Jüstel, T. On the Photoluminescence Linearity of Eu^{2+} Based LED Phosphors upon High Excitation Density. *ECS J. Solid State Sci. Technol.* **2016**, *5*, R91−R97.
(28) Yang, G.; et al. Near-Infrared Circularly Polarized Light Triggered Enantioselective Photopolymerization by Using Upconversion Nanophosphors. *Chem. - Eur. J.* **2017**, *23*, 8032−8038.
(29) Xia, Z.; Meijerink, A. Ce^{3+}-Doped garnet phosphors: composition modification, luminescence properties and applications. *Chem. Soc. Rev.* **2017**, *46*, 275−299.
(30) Trivellin, N.; et al. Laser-Based Lighting: Experimental Analysis and Perspectives. *Materials* **2017**, *10*, 1166.
(31) Ogieglo, J. M. Luminescence and Energy Transfer in Garnet Scintillators. *Ph.D. Thesis*, Utrecht University, 2012.
(32) Huang, Y.-Y.; Sharma, S. K; Carroll, J.; Hamblin, M. R Biphasic dose response in low level light therapy - an update. *Dose-Response* **2011**, *9*, 602−618.
(33) Cantore, M.; Pfaff, N.; Farrell, R. M.; Speck, J. S.; Nakamura, S.; DenBaars, S. P. High luminous flux from single crystal phosphor-converted laser-based white lighting system. *Opt. Express* **2016**, *24*, 215−221.
(34) Li, J.; et al. Advanced red phosphors for white light-emitting diodes. *J. Mater. Chem. C* **2016**, *4*, 8611−8623.
(35) Kim, Y. H.; Viswanath, N. S. M.; Unithrattil, S.; Kim, H. J.; Im, W. B. Review—Phosphor Plates for High-Power LED Applications: Challenges and Opportunities toward Perfect Lighting. *ECS J. Solid State Sci. Technol.* **2018**, *7*, R3134−R3147.
(36) Long, X.; et al. A review on light-emitting diode based automotive headlamps. *Renewable Sustainable Energy Rev.* **2015**, *41*, 29−41.
(37) George, A. F.; Al-waisawy, S.; Wright, J. T.; Jadwisienczak, W. M.; Rahman, F. Laser-driven phosphor-converted white light source for solid-state illumination. *Appl. Opt.* **2016**, *55*, 1899−1905.
(38) De Boer, D. K. G.; Bruls, D.; Jagt, H. High-brightness source based on luminescent concentration. *Opt. Express* **2016**, *24*, 1069−1074.
(39) De Boer, D. K. G.; Haenen, L. Extraction optics for high lumen density sources. *J. Eur. Opt. Soc. Publ.* **2019**, *15*, 8.
(40) Van De Haar, M. A.; et al. Increasing the effective absorption of Eu3+-doped luminescent materials towards practical light emitting diodes for illumination applications. *Appl. Phys. Lett.* **2018**, *112*, 132101.
(41) Chen, D.; Zhou, Y.; Zhong, J. A review on Mn^{4+} activators in solids for warm white light-emitting diodes. *RSC Adv.* **2016**, *6*, 86285−86296.
(42) Murphy, J. E.; Garcia-Santamaria, F.; Setlur, A. A.; Sista, S. PFS, K_2SiF_6:Mn^{4+}: the Red-line Emitting LED Phosphor behind GE's TriGain Technology Platform. *Dig. Tech. Pap. - Soc. Inf. Disp. Int. Symp.* **2015**, *46*, 927−930.
(43) Sijbom, H. F.; et al. Luminescent Behavior of the K_2SiF_6:Mn^{4+} Red Phosphor at High Fluxes and at the Microscopic Level. *ECS J. Solid State Sci. Technol.* **2016**, *5*, R3040−R3048.
(44) Adachi, S. Photoluminescence properties of Mn^{4+}-activated oxide phosphors for use in white-LED applications: A review. *J. Lumin.* **2018**, *202*, 263−281.
(45) Zhu, H.; et al. Highly efficient non-rare-earth red emitting phosphor for warm white light-emitting diodes. *Nat. Commun.* **2014**, *5*, 4312.
(46) Sijbom, H. F.; Verstraete, R.; Joos, J. J.; Poelman, D.; Smet, P. F. K_2SiF_6:Mn^{4+} as a red phosphor for displays and warm-white LEDs: a review of properties and perspectives. *Opt. Mater. Express* **2017**, *7*, 3332.
(47) Ojambati, O. S.; Yilmaz, H.; Lagendijk, A.; Mosk, A. P.; Vos, W. L. Coupling of energy into the fundamental diffusion mode of a complex nanophotonic medium. *New J. Phys.* **2016**, *18*, 043032.
(48) Nikolov, I.; et al. Optical properties of Cr^{3+}:$NaAl(WO_4)_2$ crystals, a new candidate for broadband laser applications. *Opt. Mater.* **2004**, *25*, 53−58.
(49) Wang, G.; et al. Spectroscopic characteristic and energy levels of Cr^{3+} in Cr^{3+}:$KAl(MoO_4)_2$ crystal. *J. Lumin.* **2008**, *128*, 1556−1560.
(50) Wang, G.; Zhang, L.; Lin, Z.; Wang, G. Growth and spectroscopic characteristics of Cr^{3+}:$CsAl(MoO_4)_2$ crystal. *J. Alloys Compd.* **2010**, *489*, 293−296.
(51) García-Revilla, S.; Valiente, R. F-d transitions and self-trapped excitons in $CsCdBr_3$:Eu^{2+}. *J. Phys.: Condens. Matter* **2006**, *18*, 11139−11148.
(52) Van Der Heggen, D.; Joos, J. J.; Smet, P. F. Importance of Evaluating the Intensity Dependency of the Quantum Efficiency: Impact on LEDs and Persistent Phosphors. *ACS Photonics* **2018**, *5*, 4529−4537.

https://doi.org/10.1021/acsphotonics.1c00372
ACS Photonics 2021, 8, 1784−1793

(53) Garcia-Santamaria, F.; Murphy, J. E.; Setlur, A. A.; Sista, S. P. Concentration Quenching in K_2SiF_6:Mn^{4+} Phosphors. *ECS J. Solid State Sci. Technol.* **2018**, *7*, R3030−R3033.
(54) Beers, W. W.; Smith, D.; Cohen, W. E.; Srivastava, A. M. Temperature dependence (13−600 K) of Mn^{4+} lifetime in commercial $Mg_{28}Ge_{7.55}O_{32}F_{15.04}$ and K_2SiF_6 phosphors. *Opt. Mater.* **2018**, *84*, 614−617.
(55) Senden, T.; Van Dijk-Moes, R. J. A.; Meijerink, A. Quenching of the red Mn^{4+} luminescence in Mn^{4+}-doped fluoride LED phosphors. *Light: Sci. Appl.* **2018**, *7*, 8.
(56) Miniscalco, W. J.; Pellegrino, J. M.; Yen, W. M.; et al. Measurements of excited-state absorption in Ce^{3+}:YAG. *J. Appl. Phys.* **1978**, *49*, 6109.
(57) Hamilton, D. S.; Gayen, S. K.; Pogatshnik, G. J.; Ghen, R. D.; Miniscalco, W. J. Optical-absorption and photoionization measurements from the excited states of Ce^{3+}:$Y_3Al_5O_{12}$. *Phys. Rev. B: Condens. Matter Mater. Phys.* **1989**, *39*, 8807−8815.
(58) Maiman, T. H. Stimulated Optical Radiation in Ruby. *Nature* **1960**, *187*, 493−494.
(59) Lozano, G.; et al. Plasmonics for solid-state lighting: Enhanced excitation and directional emission of highly efficient light sources. *Light: Sci. Appl.* **2013**, *2*, e66.
(60) Senden, T.; Rabouw, F. T.; Meijerink, A. Photonic effects on the radiative decay rate and luminescence quantum yield of doped nanocrystals. *ACS Nano* **2015**, *9*, 1801−1808.
(61) Aeschlimann, M.; et al. Perfect absorption in nanotextured thin films via Anderson-localized photon modes. *Nat. Photonics* **2015**, *9*, 663−668.
(62) Wang, Z.; Shen, B.; Dong, F.; Wang, S.; Su, W. S. A first-principles study of the electronic structure and mechanical and optical properties of $CaAlSiN_3$. *Phys. Chem. Chem. Phys.* **2015**, *17*, 15065−15070.

https://doi.org/10.1021/acsphotonics.1c00372
ACS Photonics 2021, 8, 1784−1793